Silicon photonic current sensor based on multimode interference

Bing Wei (魏 兵), Changyun Zhao (赵昌云), Gencheng Wang (王根成), Tingge Dai (戴庭舸), Jianyi Yang (杨建义), Kejiang Zhou (周柯江), and Yubo Li (李宇波)*

College of Information Science and Electronic Engineering, Zhejiang University, HangZhou, 310027, China
**Corresponding author: lilinear@zju.edu.cn*

Received September 23, 2015; accepted January 8, 2016; posted online February 25, 2016

We propose and demonstrate an ultrasensitive integrated photonic current sensor that incorporates a silicon-based single-mode-multimode-single-mode waveguide (SMSW) structure. This kind of SMSW structure is placed over a direct current carrying power resistor, which produces Joule's heat to change the temperature of the SMSW and further results in the change of the effective refractive index between different propagating modes. Interference occurs when the modes recombine at the second single mode waveguide. Finally, the current variation is measured by monitoring the shift in the output spectrum of the multimode interferometer. In low current, the wavelength shift has almost linear dependence: $\Delta\lambda \propto I_c$. This effect can be used as a current sensor with a slope efficiency of 4.24 nm/A in the range of 0–200 mA.

OCIS codes: 130.3120, 130.6010, 230.7380.
doi: 10.3788/COL201614.031301.

Optical current sensors have been widely discussed since the 1970s. Compared with the traditional electromagnetic induction current transformers, optical current sensors have many great advantages, such as inherent insulation, immunity to electromagnetic interference, wide dynamic range, safety, small size, and are light weight[1–3]. Generally, the conventional optical current sensors are based on Ampere's Law and the Faraday Effect; the current conductor placed in the vicinity of the sensing fiber generates a magnetic field, which rotates the polarization state of the two circularly polarized light beams passing through the sensing fiber coil. The sensitivity of the sensor is proportional to the circle number of the fiber coil and the Verdet constant of the sensing fiber. Usually, the Verdet constant of silica fiber is fairly small. Thus, to enhance the sensitivity of the sensor one needs multiple circles coiled, which induce a long piece of fiber[4,5]. However, the usage of long fiber induces a lateral variation in the transverse stress and produces undesirable thermally dependent birefringence, which may easily affect the state of polarization and affect the measurement results. Recently, many current sensors have been proposed based on the idea of measuring the thermally induced resonant wavelength shift induced by the heat dissipated by the flow of the electric current in a power resistor that touches the micro wire and micro Mach–Zehnder interferometer (MMZI)[6–10]. These sensors have the advantage of compact structure and easy integration with the fiber system; however, handling of the fiber micro wire or the tapered fibers involves complexities that result in a poor repeatability of such sensors.

Compared to the fiber sensors mentioned above, silicon photonic devices have drawn great interest from many researchers due to their remarkable advantages, like ultra-small dimensions, a flexible integration with conventional electronic integrated circuits, high sensitivity, and simple design[11–13]. A great number of integrated optical sensors based on silicon planar waveguides has been investigated in different sensing platforms, such as microring resonators[14–16], interferometers[17–19], and photonic crystals[20–22]. In this Letter, we proposed and demonstrated an ultrasensitive integrated photonic current sensor based on the principle of multimode interference. The multimode interferometer is simply a silicon-based single-mode-multimode-single-mode waveguide (SMSW) structure. The whole SMSW structure is placed over a direct current carrying power resistor, which produces Joule's heat and changes the surrounding temperature. The effective refractive index of the two modes changes with temperature and finally results in the shift of the output spectrum of the multimode interferometer. Our experiment shows that the slope efficiency of the sensor is 4.24 nm/A in the range of 0–200 mA.

The schematic structure of the proposed current sensor is shown in Fig. 1. The light from a broadband amplified spontaneous emission (ASE) source with a center wavelength of 1.55 μm, is butt-coupled into and out of the SMSW by the lensed fiber; the loss and spectral response of the interferometer is monitored by an optical spectrum analyzer (OSA) that is connected to the output end of the system. A polarization controller is used to adjust the polarization state of the input light. Figure 2(a) shows the SMSW structure, which is fabricated on silicon-on-insulator (SOI) by the CMOS compatible process in the silicon photonics platform of the Institute of Microelectronics (IME) in Singapore[23]. The designed multimode waveguide has a height of 220 nm, a width of 740 nm, and a length of $L = 2.06$ mm to support two eigenmodes;

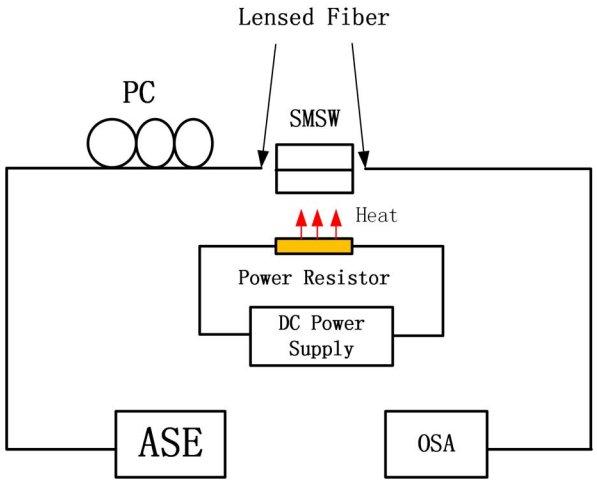

Fig. 1. Schematic of experiment setup for the proposed current sensor. PC: polarization controller.

two single mode channel waveguides with a cross section of 220 nm × 450 nm are designed on both ends of the multimode waveguide, as shown in Fig. 2(a). One is used to maximally motivate the first-order mode by a lateral displacement offset of 740/4 nm; the other one with the same offset is used to couple the two modes. The buried oxide thickness is about 3 μm. The scanning electronic microscopy (SEM) photograph of the fabricated SMSW is shown in Fig. 2(b). The simulated images of the two eigenmodes, namely the TE_0 mode and the TE_1 mode, at the cross section of the multimode waveguide are shown in Fig. 2(c). The TE_0 mode and the TE_1 mode propagate with different propagation constants through the multimode waveguide; interference occurs when the two modes recombine at the second single-mode waveguide. The transfer function of the SMSW structure can be expressed as

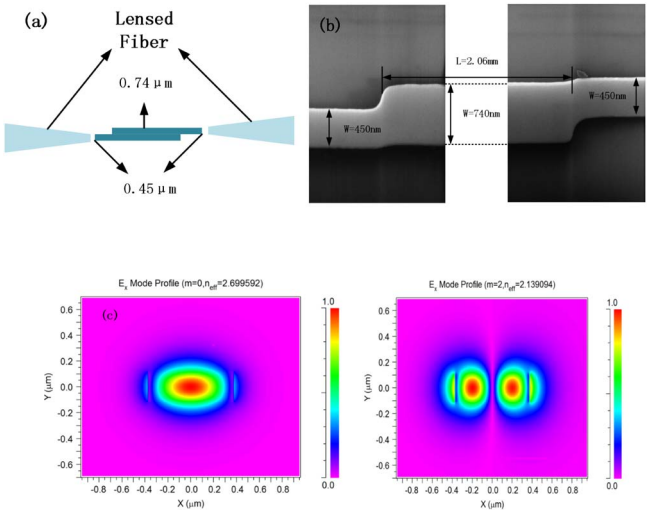

Fig. 2. (a) Schematic diagram of the butt-coupling and the designed SMSW for mode motivation using the on-chip offset launch technique. (b) The SEM photograph of the fabricated silicon-based SMSW. (c) Simulated images of the two eigenmodes.

$$I = I_0\left(1 + \cos\left(\frac{2\pi L}{\lambda}\Delta n_{\text{eff}}\_0\right)\right), \tag{1}$$

where $\Delta n_{\text{eff}}\_0 = n_{\text{eff0}} - n_{\text{eff1}}$, n_{eff0} and n_{eff1} are the effective refractive index of the TE_0 mode and TE_1 mode, respectively, L is the length of the multimode waveguide, I is the intensity of the interference signal, and I_0 is the intensity of the ASE. As the current flows through the power resistor placed under the SMSW (see Fig. 1), it dissipates heat, which increases the temperature of the waveguide and finally results in the change of the refractive index of Si due to its high thermo-optic coefficient. The refractive index change in crystalline silicon between room temperature and 550 K at the wavelength of 1523 nm is[24]

$$\frac{\partial n}{\partial T} = 9.48 \times 10^{-5} + 3.47 \times 10^{-7} \times T - 1.49 \times 10^{-10} \times T^2. \tag{2}$$

As the refractive index of Si changes, the effective refractive index of each of the two eigenmodes will change. The difference in the effective refractive index of the two modes can be rewritten as $\Delta n_{\text{eff}}\_1 = (n_{\text{eff0}} + \Delta n_{\text{eff0}}) - (n_{\text{eff1}} + \Delta n_{\text{eff1}})$ when the current flows through the power resistor, Δn_{eff0} and Δn_{eff1} denote the effective refractive index change of the two modes that is calculated by the beam propagation method (BPM) and shown in Fig. 3 with black and red lines. We can see that the effective refractive index of the TE_1 mode changes more than the TE_0 mode with the change of temperature, which leads to the spectral shift of the multimode interferometer. Based on the linear relationship between the temperature change and heat energy generated by the conducting current, the results of the change in wavelength with respect to the current/temperature are[25]

$$\frac{\Delta\lambda}{\lambda} \propto \frac{\rho I_c^2}{A}, \tag{3}$$

where ρ and A represent the conductor resistivity and the cross-sectional area of the power resistor, respectively, and

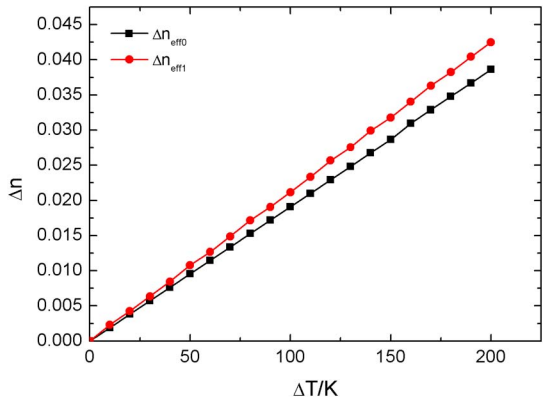

Fig. 3. Effective refractive index change of the two modes with the change of temperature, Δn_{eff0} for TE_0 mode and Δn_{eff1} for TE_1 mode.

I_c is the current. From Eq. (3), we can see that the wavelength shift changes linearly with the square of the current. However, in the case of low current sensing, there exists a good linear relationship between the current and the wavelength shift, which can be seen in Ref. [26] and will be experimentally verified in this Letter.

In the experiment, a constant current source (KEUTHLEY 2400) is used as the DC power supplier. When we are measuring the current value, 10 s settling time is given in order to get a stable wavelength shift before the spectrum is recorded. Compared with the environmental temperature variation speed, this is a short time. Therefore the environmental temperature can be regarded as a constant. Figure 4 shows the experiment result of the changes in the interference fringe spectrum of the proposed sensor in response to the change of the flowing current in the power resistor. As we can see, the fringe resonant wavelength shifts to the longer wavelength with the increase of the current. The intensity variation may be due to the presence of other modes, the presence of a coupling with the TM mode, or diffusion[27]. Figure 5 shows the wavelength shift versus the current in the range of 0–200 mA. It can be observed that a linear trend line with a correlation coefficient value of $r > 0.998$ can be fitted to the experimental data, which validates the linear relationship between the current and the wavelength shift when the current is low, as mentioned above. The experiment results also indicate a sensitivity of 4.24 nm/A for our proposed sensor in the measurement range, which is higher than previous reports[7,26]. We have nine groups of devices that were measured and each device was measured five times. The test results are quite repeatable.

The large thermo-optic coefficient of silicon leads to a huge effective refractive index change in the propagation modes when current is flowing through the power resistor; this is the reason for the ultrasensitivity property of our sensor. On the other hand, though the current sensor we proposed achieves excellent performance in the test range of 0–200 mA, the measuring range of the sensor is limited by the relatively small (about 1.5 nm) free spectral range (FSR) of the SMSW. To solve the problem of the limited measuring range, silicon-based structures that have a large FSR, such as a microring or Mach–Zehnder interferometer, can be employed.

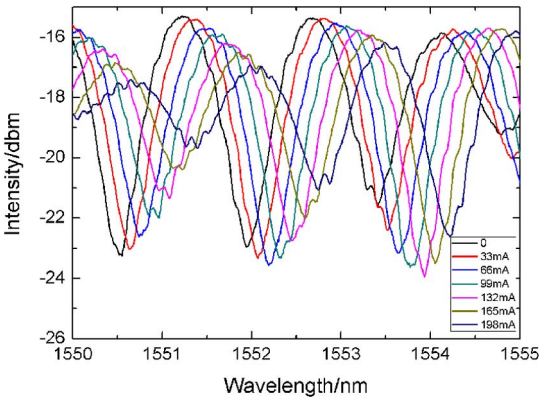

Fig. 4. Measured output spectrum versus current of the proposed sensor.

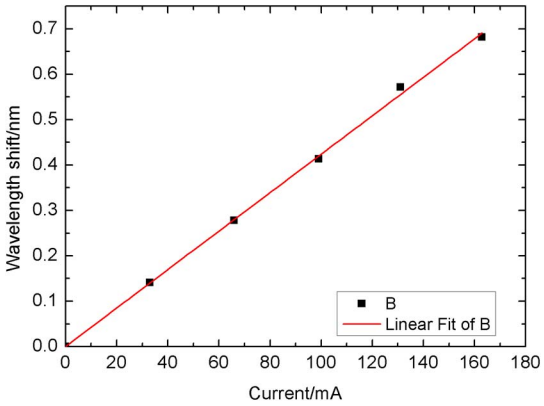

Fig. 5. Variations in the wavelength shift with current.

In conclusion, we propose and fabricate an ultrasensitive integrated photonic current sensor based on the principle of multimode interference. The current flowing through the power resistor under the silicon-based SMSW structure changes the effective refractive index of the two modes propagating in the SMSW, which results in the shift of the output spectrum of the multimode interferometer. The sensitivity of the sensor is 4.24 nm/A in the measurement range of 0–200 mA, which is much higher than that of those previously reported with optical current sensing methods. Meanwhile, a footprint of 3000 μm × 0.74 μm make the device more compact[7,26]. This sensor can be applied in areas such as electromagnetic pulse detection[28] and integrated optoelectronic interconnects[29].

This work was supported by the National 863 Project of China (No. 2015AA017001), the National Natural Science Foundation of China (Nos. 61178065, 61228501, and 61475137), and the Zhejiang Province Natural Science Foundation (No. LY14F050005).

References

1. K. Bohnert, P. Gabus, J. Nehring, and H. Brändle, J. Lightwave Technol. **20**, 267 (2002).
2. W. Wang, X. Wang, and J. Xia, Opt. Laser Technol. **43**, 1470 (2011).
3. N. Peng, Y. Huang, S. Wang, T. Wen, W. Liu, Q. Zuo, and L. Wang, IEEE Photon. Technol. Lett. **25**, 1668 (2013).
4. H. Zhang, Y. Dong, J. Leeson, L. Chen, and X. Bao, Appl Opt. **50**, 924 (2011).
5. K. Bohnert, H. Brandle, M. G. Brunzel, P. Gabus, and P. Guggenbach, IEEE Trans. Ind. Appl. **43**, 180 (2007).
6. M. Belal, Z. Q. Song, Y. Jung, G. Brambilla, and T. Newson, Opt. Express **18**, 19951 (2010).
7. A. A. Jasim, S. W. Haruna, M. Z. Muhammada, and A. H. Ahmad, Sens. Actuators A **192**, 9 (2013).
8. A. A. Jasim, S. W. Harun, H. Arof, and H. Ahmad, IEEE Sensors J. **13**, 626 (2013).
9. G. Salceda-Delgado, A. Martinez-Rios, and D. Monzón-Hernández, J. Lightwave Technol. **31**, 761 (2013).
10. L. Li, Q. Han, Y. Chen, T. Liu, and R. Zhang, IEEE Sensors J **14**, 1749 (2014).

11. Q. Xu, B. Schmidt, S. Pradhan, and M. Lipson, Nature **435**, 325 (2005).
12. W. M. J. Green, M. J. Rooks, L. Sekaric, and Y. A. Vlasov, Opt. Express **15**, 17106 (2007).
13. H. Chen, G. Wang, H. Hou, and H. Wang, Chin. Opt. Lett. **12**, 071301 (2014).
14. C. Y. Chao, W. Fung, and L. J. Guo, IEEE J. Sel. Top. Quantum Electron. **12**, 134 (2006).
15. K. De Vos, I. Bartolozzi, E. Schacht, P. Bienstman, and R. Baets, Opt. Express **15**, 7610 (2007).
16. S. Sui, M. Tang, Y. Yang, J. Xiao, Y. Du, and Y. Huang, Photon. Res. **3**, 289 (2015).
17. F. Prieto, B. Sepulveda, A. Calle, A. Llobera, C. Dominguez, A. Abad, A. Montoya, and L. M. Lechuga, Nanotechnology **14**, 907 (2003).
18. D. Hradetzky, C. Mueller, and H. Reinecke, J. Opt. A **8**, S360 (2006).
19. J. Xing, Z. Li, P. Zhou, Y. Gong, Y. Yu, M. Tan, and J. Yu, Chin. Opt. Lett. **13**, 061301 (2014).
20. Y. Zhang, J. Qiu, R. Hu, P. Li, L. Gao, L. Heng, B. Tang, and L. Jiang, Phys. Chem. Chem. Phys. **17**, 9651 (2015).
21. X. Zhang, A. Hosseini, H. Subbaraman, S. Wang, Q. Zhan, J. Luo, A. K. Y. Jen, and R. T. Chen, J. Lightwave Technol. **32**, 3774 (2014).
22. M. Lin, X. Jin, Z. Ouyang, G. Zheng, and G. Wen, Chin. Opt. Lett. **13**, S11301 (2015).
23. C. Galland, A. Novack, Y. Liu, R. Ding, M. Gould, T. Baehr-Jones, Q. Li, Y. Yang, Y. Ma, Y. Zhang, K. Padmaraju, K. Bergmen, A. E.-J. Lim, G.-Q. Lo, and M. Hochberg, Proc. SPIE **8767**, 87670G (2013).
24. G. Cocorullo, F. G. Della Corte, and I. Rendina, Appl. Phys. Lett. **74**, 3338 (1999).
25. K. S. Lim, S. S. A. Damanhuri, A. A. Jasim, H. H. Ku, S. W. Harun, and H. Ahmad, IET Optoelectron. **5**, 281 (2011).
26. K. Ramachandran, N. Kumar, and V. Sahoo, IEEE Sensors J. **15**, 1270 (2015).
27. A. Parini, P. Hamel, A. De Rossi, S. Combrie, N.-V.-Q. Tran, Y. Gottesman, R. Gabet, A. Talneau, Y. Jaouen, and G. Vadala, J. Lightwave Technol. **26**, 3794 (2008).
28. C.-Y. Lin, A. X. Wang, B. S. Lee, X. Zhang, and R. T. Chen, Opt. Express **19**, 17372 (2011).
29. H. Subbaraman, X. Xu, A. Hosseini, X. Zhang, Y. Zhang, D. Kwong, and R. T. Chen, Opt. Express **23**, 2487 (2015).